Communication

A Controlled Reception Pattern Antenna Array With Dual-Mode Circular Microstrip Antenna Elements for Increased Angular Availability

Navid Rezazadeh and Lotfollah Shafai

***Abstract*— Planar-controlled reception pattern antenna (CRPA) arrays suffer from low null resolution at low elevation angles, which results in a diminished angular space available for reception. The null resolution becomes even worse as the array aperture size is shrunk in modern compact CRPAs. Nonplanar arrays have been used to address this issue, but they are high profile and bulky. A novel planar solution, specifically suited for compact arrays, is proposed in this communication. We show that by utilizing concentric dual-mode TM_{11}–TM_{21} circular microstrip antenna elements in an array, an angular availability similar to a spherical array can be achieved. This is demonstrated by studying the array nulling performance in many Monte Carlo trials with randomly polarized interferers, where the adapted array patterns are computed using a simple null-steering algorithm.**

***Index Terms*— Controlled reception pattern antenna, global navigation satellite systems, interference suppression, microstrip antennas.**

I. Introduction

Radio frequency interference (RFI) is one of the main threats to the global navigation satellite system (GNSS) receivers. Controlled reception pattern antenna (CRPA) arrays are very effective in mitigating the problem by spatially filtering the desired signal based on an adaptive algorithm [1]. As such, the radiation pattern of a CRPA is adapted to place nulls in the direction of the incident interfering plane waves.

One of the performance measures of a CRPA is the angular availability, i.e., the portion of the angular space with an output signal-to-interference-and-noise ratio (SINR) above a threshold value, obtained after the pattern is adapted to suppress the interferers. A better angular coverage, particularly for low-elevation angle satellites, is essential for a higher dilution of precision and therefore better accuracy of positioning, since the ideal scenario for a receiver is when it can receive the navigation data from one satellite at zenith and three others distributed uniformly at horizon [2].

Among different CRPAs, planar arrays of microstrip antennas (MSAs) are suitable for many GNSS applications [3]. Such arrays usually consist of several elements (<10), all working in the dominant mode with broadside radiation patterns. The angular availability of such arrays, however, degrades for low-elevation angle interferers due to the low null resolution. It is also known that the smaller the aperture size of a planar array is, the lower the null resolution and that the null resolution cannot be improved by increasing the number of the antenna elements for a fixed aperture size [4].

Given that most modern planar CRPA array designs are extremely compact, with very small apertures (e.g., 3.5" four-element arrays in [3]) and element separations much smaller than half a wavelength, the issue of low angular availability becomes increasingly important.

The attempts to increase the angular availability have been focused mostly on nonplanar arrays [5]–[7]. An array conformal to a spherical surface was investigated in [5], where the effect of the surface curvature was studied on the array nulling performance, and it was shown that the most uniform average output SINR in the elevation plane is achieved for a hemispherical array geometry. The power minimization method with a nondirectional constraint was used as the processing technique in [5]. A similar study was done in [6] in which the effects of various aspects of the geometry of a nonplanar array on its performance were investigated using the power minimization method with both the directional and nondirectional constraints, and it was concluded that a hemispherical array with elements distributed uniformly on its surface is the optimum geometry. In a different approach in [7], a uniform circular array (UCA) was split into two subarrays, which were then placed on a spherical surface. Each subarray was, however, flat and not conformal to the hemisphere. The performance of the array was studied for a least-mean-square adaptive processor, and some improvements in the null depth and null width were achieved.

Despite the good performance of nonplanar arrays, they are not low profile and therefore not suitable for many applications such as airborne receivers. The aim of this communication is to investigate a new approach to improving the angular availability of compact planar arrays without resorting to nonplanar geometries.

The angular availability of an adaptive array, aside from the spatial distribution of the phase centers of the elements (which also determines the physical aperture size), and the adaptive processing technique, to some extent, also depend on the element radiation patterns [8]–[10]. It is, e.g., known that the angular availability of an array with dissimilar element radiation patterns could be very different from that of the same array but with identical element radiation patterns.

The dissimilarity in the element radiation patterns may be achieved by pointing physically identical elements in different directions, which is the case in nonplanar arrays, or by using physically different antenna elements in the array. In this communication, we take the latter approach and employ dual-mode circular MSAs to achieve the pattern dissimilarity.

To this end, we investigate the use of dual-mode TM_{11}–TM_{21} circular MSAs in an array configuration. The TM_{n1} modes have been previously used in concentric multimode configurations for null steering and beamforming in the upper hemisphere in [11]–[13]. Arrays of such multimode elements have been studied for the multiple-input multiple-output applications, e.g., in [14], to achieve pattern diversity, but the performance of such arrays for GNSS null steering is unknown and is, therefore, the subject of study in this communication.

This communication is organized as follows. In Section II, first, we review the theoretical radiation characteristics of circular MSAs for the first two TM_{n1} modes and then present the three array

Manuscript received March 22, 2017; revised December 7, 2017; accepted January 29, 2018. Date of publication February 9, 2018; date of current version May 3, 2018. *(Corresponding author: Lotfollah Shafai.)*

The authors are with the Department of Electrical and Computer Engineering, University of Manitoba, Winnipeg, MB R3T 5V6, Canada (e-mail: rezazadn@myumanitoba.ca; l.shafai@umanitoba.ca).

Color versions of one or more of the figures in this communication are available online at http://ieeexplore.ieee.org.

Digital Object Identifier 10.1109/TAP.2018.2804619

configurations to be studied in this work: 1) a planar array of dominant TM_{11} mode elements, representing the conventional CRPA design; 2) a spherical array of dominant TM_{11} mode elements, representing the improved CRPA design; and 3) a novel planar array consisting of dual-mode TM_{11}–TM_{21} circular microstrip antenna elements. To compare the null-steering performance of the arrays in the CRPA mode, a Monte Carlo approach is adopted, in which many trials with random RFI incident angles are performed. The steady state adapted patterns of the arrays in the presence of RFI are found using the analytical expressions for the radiation patterns of the antenna elements and a least square method for pattern synthesis with null constraints. The null-steering performance evaluation method is fully detailed in Section III, and the results of the Monte Carlo simulations are presented in Section IV.

II. Arrays of Circular MSA Elements

The radiation characteristics of the TM_{n1} mode circular MSAs are reviewed in this section, and the geometry of three array configurations consisting of such elements is presented. In this work, we assume that the antenna elements are printed on thin substrates with infinite ground planes, and ignore the antenna losses and mutual coupling effects in the arrays.

The linearly polarized (LP) radiated field of a circular MSA, placed at the origin at the $z = 0$ plane and fed at $\phi = 0$, for the TM_{n1} mode is given as [15]

$$\vec{E}_n(\theta, \varphi) = E_0[f_n(\theta)\cos n\varphi\vec{\theta} + g_n(\theta)\sin n\varphi\vec{\varphi}] \tag{1}$$

where E_0 is a constant and the functions f_n and g_n, for an infinite ground plane, are

$$\begin{cases} f_n(\theta) = [J_{n+1}(k_0 a_n \sin\theta) - J_{n-1}(k_0 a_n \sin\theta)] \\ g_n(\theta) = [J_{n+1}(k_0 a_n \sin\theta) + J_{n-1}(k_0 a_n \sin\theta)]\cos\theta \end{cases} \tag{2}$$

where $J_n(x)$ is the Bessel function of order n, k_0 is the propagation constant in free space, and a_n is the patch's effective radius. For a finite ground plane, the shape and size of the ground plane also affect f_n and g_n [16]. The finite ground plane effects are ignored in this section.

Another LP pattern orthogonal in polarization to (1) can be achieved by feeding the patch from an angle $\varphi_n = \pi/2n$ from the first feed, which gives a radiated field

$$\vec{E}_n(\theta, \varphi - \varphi_n) = E_0'[f_n(\theta)\sin n\varphi\vec{\theta} - g_n(\theta)\cos n\varphi\vec{\varphi}]. \tag{3}$$

This second LP pattern can either be used in quadrature phase along with (1) to produce circularly polarized (CP) radiation, or taken as an independent channel in a polarimetric array. When $E_0' = -jE_0$, RHCP is the dominant polarization component in the upper hemisphere given as

$$E_n^{\mathrm{RHCP}}(\theta, \varphi) = \frac{E_0}{\sqrt{2}}[f_n(\theta) - g_n(\theta)]e^{-jn\varphi} \tag{4}$$

and the cross polarization is

$$E_n^{\mathrm{LHCP}}(\theta, \varphi) = \frac{E_0}{\sqrt{2}}[f_n(\theta) + g_n(\theta)]e^{jn\varphi}. \tag{5}$$

The TM_{n1} modes are orthogonal to one another, and therefore, multiple modes can radiate from the same phase center. For a fixed interelement spacing, an array of multimode elements has more ports compared with a conventional array of dominant mode elements [17] and therefore more degrees of freedom for nulling.

To construct an array with dual-mode TM_{11}–TM_{21} elements, first, the dimensions of the elements have to be determined. For the analysis in this section, we assume that both modes in a dual-mode element radiate from the same phase center. In practice, this is valid for a stacked configuration with a negligible substrate thickness, or if the TM_{21} mode is radiated by a ring patch in which case the array structure becomes entirely coplanar. For a substrate with a dielectric relative permittivity of ϵ_r, the ratio of the patch effective radius to the free space wavelength is [15]

$$\frac{a_n}{\lambda_0} = \frac{\chi_{n1}}{2\pi\sqrt{\epsilon_r}} \tag{6}$$

where χ_{n1} is the first zero of $J_n'(k_0 r)$. To use the TM_{11} and TM_{21} mode elements in a compact array, the substrate permittivity is chosen as $\epsilon_r = 9.8$ (Rogers TMM10), with given $\chi_{11} = 1.84$ and $\chi_{21} = 3.05$, results in patch radii of $a_1 = 0.09\lambda_0$ and $a_2 = 0.16\lambda_0$ for the first and second modes, respectively. The radiation patterns of these two modes are shown in Fig. 1. The plots show the upper hemisphere only and are in polar format (the center of the plot represents zenith and the perimeter represents the horizon).

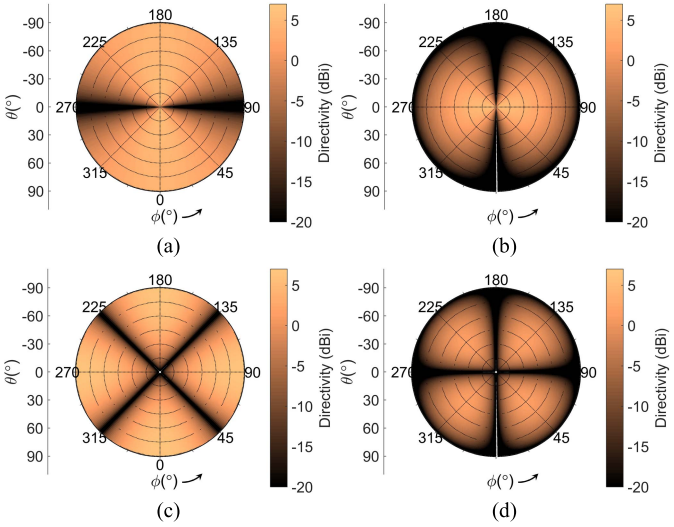

Fig. 1. Directivity patterns of the TM_{11} and TM_{21} circular MSAs assuming $\epsilon_r = 9.8$ and infinite ground plane. (a) $D_\theta^{\mathrm{TM}_{11}}$. (b) $D_\varphi^{\mathrm{TM}_{11}}$. (c) $D_\theta^{\mathrm{TM}_{21}}$. (d) $D_\varphi^{\mathrm{TM}_{21}}$.

Three different array configurations are considered, as depicted in Fig. 2. Fig. 2(a) shows a planar UCA with nine CP TM_{11} patches. Such an array has been shown to be the optimum configuration in a planar geometry [10]. The second array, shown in Fig. 2(b), is a spherical array of nine CP TM_{11} elements, with one element at the top and the others distributed uniformly on the equator. The third array, shown in Fig. 2(c), consists of three dual-mode TM_{11}–TM_{21} elements. The TM_{11} mode is excited for CP radiation, while the two orthogonal polarizations of the TM_{21} mode are used independently in order to achieve the same number of degrees of freedom as the other two arrays.

In all three array geometries of Fig. 2, the total number of array ports is nine, resulting in eight degrees of freedom for nulling. Furthermore, the elements have been distributed such that the maximum footprint of all three arrays have a diameter of λ_0.

III. Array Null-Steering Performance Evaluation Method

In general, the performance of an adaptive array is dependent on both the spatial and temporal filtering. The time-domain filtering in a space–time adaptive processor (STAP) is essential to account for dispersive antenna and radio frequency (RF) front-end, as well as the adverse effects of the couplings, particularly when suppressing wideband interferers [18], [19]. It has, however, been

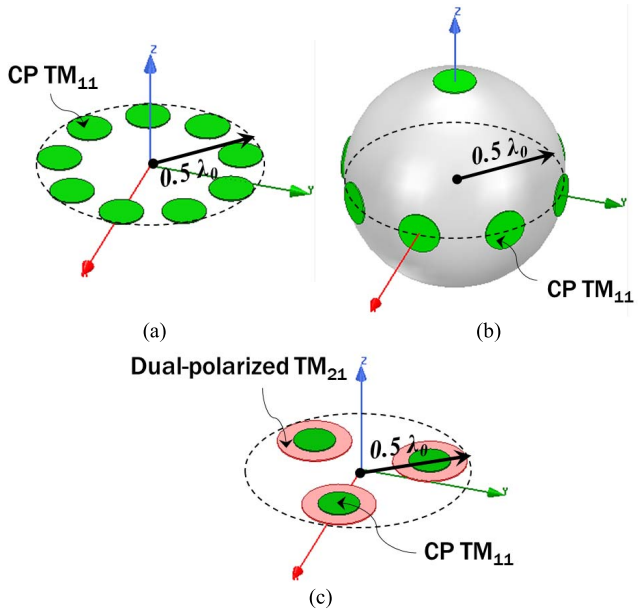

Fig. 2. Three array configurations are studied. All arrays have nine ports. (a) UCA of nine CP TM_{11} antenna elements. (b) Spherical array of nine CP TM_{11} elements. (c) Array with three dual-mode TM_{11}–TM_{21} elements.

shown that when evaluating the angular availability of an adaptive array, the performance of an STAP in the presence of wideband signals is similar to that of a space-adaptive processor (SAP) in the presence of continuous wave (CW) signals [10]. Since the aim of this communication is to study the effects of the element patterns on the performance, we consider SAP in the presence of CW desired and RFI signals. The results are, however, applicable to the wideband case, provided that time filtering is added to the array. Furthermore, it is assumed that the arrays are small, such that the time delays experienced by the signals reaching different array elements can be modeled as simple phase shifts [20].

To evaluate the performance of each array, a series of trials are run in MATLAB. In each trial, J number of RFI plane waves are incident from angular directions $(\theta_{ij}, \varphi_{ij})$, $j = 1, 2, \ldots, J$, where θ_{ij} is randomized from [60°, 90°] and φ_{ij} is randomized from [0°, 360°], with uniform probability distribution for the solid angles in the 0° to 30° elevation angle region, which is the region where the RFIs most likely originate from in practice. A random polarization and a phase are assigned to the jth interferer with a unit-amplitude polarization-phase vector of the form $\hat{e}_{ij} = e^{j\psi_{ij}}(\sqrt{1-\rho_{ij}^2}\hat{\theta} + e^{j\delta_{ij}}\rho_{ij})\hat{\varphi}$, where ρ_{ij} is the amplitude ratio between the two orthogonal polarization components and is chosen from [0, 1] interval, δ_{ij} is the phase difference between the two orthogonal polarization components chosen from $[0, 2\pi]$, and ψ_{ij} is the carrier phase chosen from $[0, 2\pi]$, all with uniform probability distributions.

An adaptive algorithm is required to compute the weight vector of an adaptive array and to update it as the new data are received in real time. However, to simplify the analysis here, we only consider the steady-state behavior of the adaptive arrays.

The steady state weights are found using the method described in [20, pp. 166–170], in which for an antenna array with N ports, the complex weight vector $\mathbf{w} \in \mathbb{C}^{N\times 1}$ is found as the best approximation to a desired weight vector $\mathbf{w}_0$ subject to the null constraints. This is stated as

$$\mathbf{w} = \arg\min_{\mathbf{w}} \|\mathbf{w} - \mathbf{w_0}\|^2, \quad \text{s.t. } \mathbf{w}^H\mathbf{U_i} = 0 \tag{7}$$

where the superscript H denotes a Hermitian transpose and $\mathbf{U_i} \in \mathbb{C}^{N\times J}$ is a matrix whose columns are the array's response vectors in the direction of the RFIs written as

$$\mathbf{U_i} = [\mathbf{u}_{i1} \vdots \mathbf{u}_{i2} \vdots \cdots \vdots \mathbf{u}_{iJ}] \tag{8}$$

where the jth column is

$$\mathbf{u}_{ij} = \begin{bmatrix} U_1(\theta_{ij}, \phi_{ij}, \hat{e}_{ij}) \\ U_2(\theta_{ij}, \phi_{ij}, \hat{e}_{ij}) \\ \vdots \\ U_N(\theta_{ij}, \phi_{ij}, \hat{e}_{ij}) \end{bmatrix} \tag{9}$$

where

$$U_m(\theta_{ij}, \phi_{ij}, \hat{e}_{ij}) = e^{j\vec{k}_{ij}\cdot\vec{p}_m}\sqrt{G_m(\theta_{ij}, \phi_{ij})}\hat{e}_m(\theta_{ij}, \phi_{ij}) \cdot \hat{e}_{ij} \tag{10}$$

where $\vec{p}_m$, $G_m(\theta, \varphi)$, and $\hat{e}_m(\theta, \varphi)$ are the position, gain pattern, and the polarization-phase vector of the mth element of the array, respectively, and $\vec{k}_{ij}$ is the wavenumber of the jth incident interference plane wave, which is given as

$$\vec{k}_{ij} = \frac{2\pi}{\lambda_0}(\sin\theta_{ij}\cos\phi_{ij}\hat{x} + \sin\theta_{ij}\sin\phi_{ij}\hat{y} + \cos\theta_{ij}\hat{z}). \tag{11}$$

For the analysis in this section, G_m and $\hat{e}_m$ are computed from (1)–(5). The effects of coupling and antenna losses are, therefore, ignored.

The solution to (7) is given as

$$\mathbf{w} = \left[\mathbf{I}_N - \mathbf{U}_i(\mathbf{U}_i^H\mathbf{U}_i)^{-1}\mathbf{U}_i^H\right]^H\mathbf{w}_0 \tag{12}$$

where $\mathbf{I}_N$ is the identity matrix and the desired weight vector is chosen to be $\mathbf{w}_0 = [1\ 0\ \ldots\ 0]^T$ here, i.e., the desired pattern is assumed to be the quiescent pattern of the array, which is produced when only the reference element is active. A processor utilizing this constraint is referred to as "simple null-steering" adaptive processor in [4]. This simple constraint is useful for practical applications, where the direction of the desired signal is not known. Since no *a priori* knowledge of the satellite direction is used, the weights can be applied to all the satellites in view, making this method suitable for single-output adaptive processors [1], [4].

The selection of the reference element for the planar array of Fig. 2(a) is arbitrary because of the symmetry. For the spherical array of Fig. 2(b), the top element is selected as the reference element and for the dual-mode array of Fig. 2(c), one of the TM_{11} elements is selected to be the reference element.

To evaluate the angular space available for reception, after the pattern is adapted, the SINR level at the output of the adaptive array is used as the criteria. A single desired signal is assumed to be incident on the array from (θ_d, ϕ_d) and the plane wave associated with it is assumed to be RHCP. The appropriate polarization-phase vector for the incident desired signal is, therefore, $\hat{e}_d = e^{i\psi_d}(\hat{\theta} + j\hat{\varphi})/\sqrt{2}$, where ψ_d is chosen from $[0, 2\pi]$ with uniform probability distribution. Assuming that the desired and RFI signals are uncorrelated and stationary, and that the white noise at different input ports are also uncorrelated, the output SINR is given as

$$\text{SINR}_{\text{out}} = \frac{\mathbf{w}^H\mathbf{R}_d\mathbf{w}}{\mathbf{w}^H(\mathbf{R}_i + \sigma^2\mathbf{I}_N)\mathbf{w}} \tag{13}$$

where $\mathbf{R}_d$ and $\mathbf{R}_i$ are the desired signal and interference covariance matrices (which are equal to the spatial spectral matrices for CW signals in a space–time random process [20]) and σ^2 is the noise power. $\mathbf{R}_d$ is given as

$$\mathbf{R}_d = \mathbf{u}_d A_d^2 \mathbf{u}_d^H \tag{14}$$

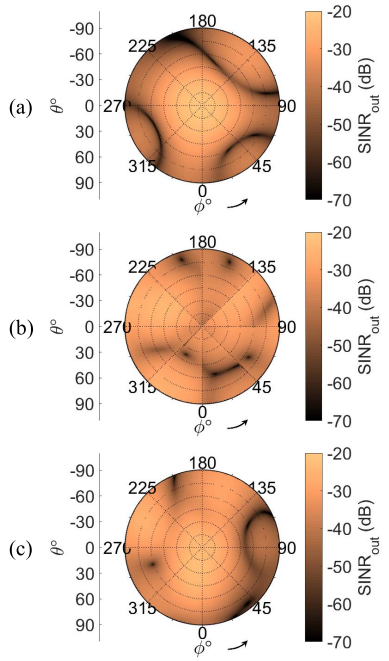

Fig. 3. Output SINR of the three arrays of Fig. 2, assuming seven randomly polarized RFIs at angles (60°, 30°), (70°, 60°), (75°, 100°), (80°, 195°), (85°, 200°), (60°, 290°), and (60°, 300°). The input SINR is −80 dB. (a) Planar TM_{11} UCA of Fig. 2(a). Availability for $SINR_{thr} = -30$ dB is 29%, and for $SINR_{thr} = -35$ dB is 47%. (b) Spherical TM_{11} array of Fig. 2(b). Availability for SINR_thr = −30 dB is 33%, and for $SINR_{thr} = -35$ dB is 67%. (c) Planar dual-mode TM_{11}–TM_{21} array of Fig. 2(c). Availability for SINR_thr = −30 dB is 41%, and for SINR_thr = −35 dB is 65%.

where $\mathbf{u}_d$ is the array response vector to the desired signal plane wave, and similar to (9) is given as

$$\mathbf{u}_d = \begin{bmatrix} U_1(\theta_d, \phi_d, \hat{e}_d) \\ U_2(\theta_d, \phi_d, \hat{e}_d) \\ \vdots \\ U_N(\theta_d, \phi_d, \hat{e}_d) \end{bmatrix} \tag{15}$$

and A_d is the desired signal amplitude. The interference covariance matrix $\mathbf{R}_i$ can be written as

$$\mathbf{R}_i = \mathbf{U}_i \mathbf{S}_i \mathbf{U}_i^H \tag{16}$$

where $\mathbf{U}_i$ is given in (8) and $\mathbf{S}_i \in \mathbb{R}^{J\times J}$ is the frequency spectral matrix of the interference sources and since the RFIs are assumed to be uncorrelated with one another, it is a diagonal matrix $\text{diag}(A_{i1}^2, A_{i2}^2, \ldots, A_{iN}^2)$, whose elements are the RFI powers. For the current analysis, we assume that $A_d^2/\sigma^2 = 10^{-3}$ and $A_{ij}^2/\sigma^2 = 10^5$ for $j = 1, 2, \ldots, J$, i.e., the desired signal is assumed to be 30 dB below noise and the RFIs are assumed to be 50 dB above noise level at the input of the adaptive array (for isotropic elements). These values are typical in GNSS antijamming array studies [6].

Finally, to characterize each array in terms of its angular available space with an acceptable output SINR, in each trial, the desired signal direction (θ_d, ϕ_d) is swept over the entire upper hemisphere (in 1° steps in both elevation and azimuth) and the output SINR is calculated using (13) for each angle.

The angular availability is defined as the portion of the upper hemisphere, where the output SINR exceeds a threshold level as

$$\text{Ang. Av.} = \int_{\phi_d=0}^{2\pi} \int_{\theta_d=0}^{\pi/2} \frac{1}{4\pi} [\text{sgn}(\text{SINR}_{\text{out}} - \text{SINR}_{\text{thr}}) + 1] \times \sin(\theta_d) d\theta_d d\varphi_d. \tag{17}$$

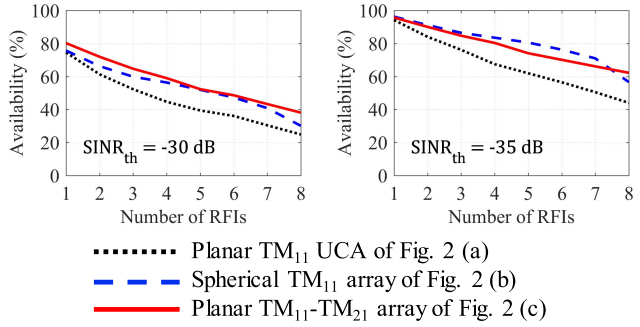

Fig. 4. Angular availability of the arrays of Fig. 2 for different numbers of randomly polarized RFIs.

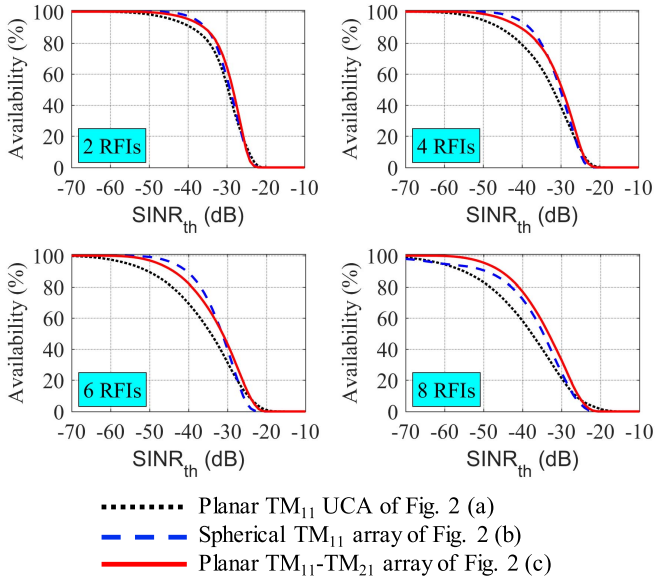

Fig. 5. Angular availability of the arrays of Fig. 2, plotted as a function of SINR_thr, for various numbers of RFIs.

IV. Analysis Results

The analysis of part B was performed for the three arrays of Fig. 2 over 100 trials. The output SINR in the upper hemisphere in a single trial is shown in Fig. 3, when seven interferers are incident. The availability values are given for two $SINR_{thr}$ values of −30 and −35 dB in this case. Note that $SINR_{thr} = -30$ dB $= SNR_{in}$ is the ideal situation where the interferers have been completely suppressed. $SINR_{thr} = -35$ dB, on the other hand, is the situation where a 5 dB degradation in SNR_{in} is allowed. In general, the exact value of the $SINR_{thr}$ will depend on the application. Moving platforms, e.g., require a higher threshold value compared to static platforms [2].

Fig. 4 shows the results of the nulling performance study of the arrays, when averaged over all 100 trials. As it can be seen, the proposed array of dual-mode TM_{11}–TM_{21} elements performs significantly better than the planar TM_{11} UCA and very similar to the spherical TM_{11} array. This is remarkable since this array is entirely planar and has the same footprint as the spherical array.

Since as mentioned, the exact value of $SINR_{thr}$ will depend on the application, the angular availability results are given in Fig. 5 as a function of $SINR_{thr}$, for various numbers of interferers. The results clearly show the significant improvement achieved by the array of dual-mode TM_{11}–TM_{21} elements compared to the planar TM_{11} UCA, especially as the number of interferers increases.

V. Conclusion

With the aim of improving the angular availability of planar CRPAs, an array of dual-mode circular MSA elements, where each element radiates a CP TM_{11} pattern and two orthogonal LP TM_{21} patterns was proposed and studied. The nulling performance of the array was evaluated by performing many Monte Carlo trials with randomly polarized interferers, where the adapted pattern of the array was computed using a nondirectional constrained adaptive algorithm. It was shown that the angular availability of the proposed dual-mode array is significantly better than a conventional planar CRPA with TM_{11} elements and similar to a spherical CRPA with TM_{11} elements.

References

[1] C. Fernández-Prades, J. Arribas, and P. Closas, "Robust GNSS receivers by array signal processing: Theory and implementation," *Proc. IEEE*, vol. 104, no. 6, pp. 1207–1220, Jun. 2016.

[2] B. R. Rao, W. Kunysz, R. Fante, and K. McDonald, *GPS/GNSS Antennas*. Norwood, MA, USA: Artech House, 2012.

[3] J. L. Volakis, A. J. O'Brien, and C.-C. Chen, "Small and adaptive antennas and arrays for GNSS applications," *Proc. IEEE*, vol. 104, no. 6, pp. 1221–1232, Jun. 2016.

[4] I. J. Gupta, I. M. Weiss, and A. W. Morrison, "Desired features of adaptive antenna arrays for GNSS receivers," *Proc. IEEE*, vol. 104, no. 6, pp. 1195–1206, Jun. 2016.

[5] J. R. Lambert, C. A. Balanis, and D. DeCarlo, "Spherical cap adaptive antennas for GPS," *IEEE Trans. Antennas Propag.*, vol. 57, no. 2, pp. 406–413, Feb. 2009.

[6] I. J. Gupta *et al.*, "Non-planar adaptive antenna arrays for GPS receivers," *IEEE Antennas Propag. Mag.*, vol. 52, no. 5, pp. 35–51, Oct. 2010.

[7] G. Byun, H. Choo, and S. Kim, "Improvement of pattern null depth and width using a curved array with two subarrays for CRPA systems," *IEEE Trans. Antennas Propag.*, vol. 63, no. 6, pp. 2824–2827, Jun. 2015.

[8] I. J. Gupta and A. A. Ksienski, "Prediction of adaptive array performance," *IEEE Trans. Aerosp. Electron. Syst.*, vol. AES-19, no. 3, pp. 380–388, May 1983.

[9] R. T. Compton, Jr., "On eigenvalues, SINR, and element patterns in adaptive arrays," *IEEE Trans. Antennas Propag.*, vol. AP-32, no. 6, pp. 643–647, Jun. 1984.

[10] J. A. Ulrey and I. J. Gupta, "Optimum element distribution for circular adaptive antenna systems," in *Proc. Inst. Navigat. Nat. Tech. Meeting*, Jan. 2006, pp. 76–81.

[11] L. Shafai, "Linear-sum mode arrays and beam forming," in *Proc. Symp. Antenna Technol. Appl. Electromagn.*, Winnipeg, MB, Canada, Aug. 1992, pp. 57–62.

[12] T. Q. Tran and S. K. Sharma, "Radiation characteristics of a multimode concentric circular microstrip patch antenna by controlling amplitude and phase of modes," *IEEE Trans. Antennas Propag.*, vol. 60, no. 3, pp. 1601–1605, Mar. 2012.

[13] N. R. Labadie, S. K. Sharma, and G. M. Rebeiz, "A circularly polarized multiple radiating mode microstrip antenna for satellite receive applications," *IEEE Trans. Antennas Propag.*, vol. 62, no. 7, pp. 3490–3500, Jul. 2014.

[14] T. Svantesson, "Correlation and channel capacity of MIMO systems employing multimode antennas," *IEEE Trans. Veh. Technol.*, vol. 51, no. 6, pp. 1304–1312, Nov. 2002.

[15] J. Huang, "Circularly polarized conical patterns from circular microstrip antennas," *IEEE Trans. Antennas Propag.*, vol. AP-32, no. 9, pp. 991–994, Sep. 1984.

[16] S. I. Latif and L. Shafai, "Pattern equalization of circular patch antennas using different substrate permittivities and ground plane sizes," *IEEE Trans. Antennas Propag.*, vol. 59, no. 10, pp. 3502–3511, Oct. 2011.

[17] N. R. Labadie, S. K. Sharma, and G. M. Rebeiz, "Investigations on the use of multiple unique radiating modes for 2-D beam steering," *IEEE Trans. Antennas Propag.*, vol. 64, no. 11, pp. 4659–4670, Nov. 2016.

[18] I. J. Gupta, J. A. Ulrey, and E. H. Newman, "Effects of antenna element bandwidth on adaptive array performance," *IEEE Trans. Antennas Propag.*, vol. 53, no. 7, pp. 2332–2336, Jul. 2005.

[19] A. S. C. Svendsen and I. J. Gupta, "The effect of mutual coupling on the nulling performance of adaptive antennas," *IEEE Antennas Propag. Mag.*, vol. 54, no. 3, pp. 17–38, Jun. 2012.

[20] H. L. Van Trees, *Detection, Estimation, and Modulation Theory, Optimum Array Processing*. Hoboken, NJ, USA: Wiley, 2004.

[21] S. Maddio, A. Cidronali, and G. Manes, "A new design method for single-feed circular polarization microstrip antenna with an arbitrary impedance matching condition," *IEEE Trans. Antennas Propag.*, vol. 59, no. 2, pp. 379–389, Feb. 2011.